Peculiar behaviour of optical polarization gratings in light-sensitive liquid crystalline elastomers

Matej Prijatelj,[1] Mostafa A. Ellabban,[2,3] Martin Fally,[4,*] Valentina Domenici,[5] Martin Čopič,[1,6] and Irena Drevenšek-Olenik[1,6]

[1]*J. Stefan Institute, Jamova 39, SI 1000 Ljubljana, Slovenia*
[2]*Physics Department, Faculty of Science, Tanta University, Tanta 31527, Egypt*
[3] *Physics Department, Faculty of Science, Taibah University, Al-Madina Al-Monaoura, P.O. Box 30002, Saudi Arabia*
[4]*Faculty of Physics, University of Vienna, Boltzmanngasse 5, A-1090 Wien, Austria*
[5]*Dipartimento di Chimica e Chimica Industriale, University of Pisa, via Moruzzi 3, 56124 Pisa, Italy*
[6]*Faculty of Mathematics and Physics, University of Ljubljana, Jadranska 19, SI 1000 Ljubljana, Slovenia*
[*]*Martin.Fally@univie.ac.at*

Abstract: The angular dependence of the diffraction efficiency of volume-type holographic gratings recorded in a single-domain light-sensitive liquid crystalline elastomer was investigated. Usually this dependence is expected to be very similar for intensity gratings and for polarization gratings. However, our measurements resolved a profound difference between the two types of the gratings: a typical Bragg peak of the diffraction efficiency is observed only for intensity gratings, while polarization gratings exhibit a profound dip at the Bragg angle. The appearance of this dip is explained by strongly anisotropic optical absorption of the actinic light during the recording process.

OCIS codes: (050.1950) Diffraction gratings; (050.1930) Dichroism; (160.5335) Photosensitive materials.

References and links

1. T. Todorov, L. Nikolova, and N. Tomova, "Polarization holography. 1: A new high-efficiency organic material with reversible photoinduced birefringence," Appl. Opt. **23**(23), 4309–4312 (1984).
2. T. Todorov, L. Nikolova, and N. Tomova, "Polarization holography. 2: Polarization holographic gratings in photoanisotropic materials with and without intrinsic birefringence," Appl. Opt. **23**(24), 4588–4591 (1984).
3. T. Todorov, L. Nikolova, K. Stoyanova, and N. Tomova, "Polarization holography. 3: Some applications of polarization holographic recording," Appl. Opt. **24**(6), 785–788 (1985).
4. C. Oh and M. J. Escuti, "Achromatic diffraction from polarization gratings with high efficiency," Opt. Lett. **33**(20), 2287–2289 (2008).
5. X. Pan, C. Wang, C. Wang, and X. Zhang, "Image storage based on circular-polarization holography in an azobenzene side-chain liquid-crystalline polymer," Appl. Opt. **47**(1), 93–98 (2008).
6. S. R. Nersisyan, N. V. Tabiryan, L. Hoke, D. M. Steeves, and B. R. Kimball, "Polarization insensitive imaging through polarization gratings," Opt. Express **17**(3), 1817–1830 (2009).
7. S. H. Lin, S. L. Cho, S. F. Chou, J. H. Lin, C. M. Lin, S. Chi, and K. Y. Hsu, "Volume polarization holographic recording in thick photopolymer for optical memory," Opt. Express **22**(12), 14944–14957 (2014).
8. A. Shishido, "Rewritible holograms based on azobenzene-containing liquid-cystalline polymers," Polym. J. **42**(7), 525–533 (2010).
9. H. Yu, "Recent advances in photoresponsive liquid-crystalline polymers containing azobenzene chromophores," J. Mater. Chem. C Mater. Opt. Electron. Devices **2**(17), 3047–3054 (2014).
10. N. Kawatsuki, A. Yamashita, M. Kondo, T. Matsumoto, T. Shioda, A. Emoto, and H. Ono, "Photoinduced reorientation and polarization holography in photo-cross-linkable liquid crystalline polymer films with large birefringence," Polymer (Guildf.) **51**(13), 2849–2856 (2010).
11. T. Sasaki, T. Shoho, K. Goto, K. Noda, N. Kawatsuki, and H. Ono, "Photoalignment and resulting holographic vector grating formation in composites of low molecular weight liquid crystals and photoreactive liquid crystalline polymers," Appl. Phys. B **120**(2), 217–222 (2015).
12. X. Pan, C. Wang, H. Xu, C. Wang, and X. Zhang, "Polarization holographic gratings in an azobenzene side-chain liquid-crystalline polymer," Appl. Phys. B **86**(4), 693–697 (2007).
13. S. P. Gorkhali, S. G. Cloutier, G. P. Crawford, and R. A. Pelcovits, "Stable polarization gratings recorded in azo-dye-doped liquid crystals," Appl. Phys. Lett. **88**(25), 251113 (2006).

#258431 Received 28 Jan 2016; revised 15 Feb 2016; accepted 15 Feb 2016; published 29 Feb 2016

14. V. Presnyakov, K. Asatryan, T. Galstian, and V. Chigrinov, "Optical polarization grating induced liquid crystal micro-structure using azo-dye command layer," Opt. Express **14**(22), 10558–10564 (2006).
15. C. Provenzano, P. Pagliusi, and G. Cipparrone, "Highly efficient liquid crystal based diffraction grating induced by polarization holograms at the aligning surfaces," Appl. Phys. Lett. **89**(12), 121105 (2006).
16. B. J. Kim, S. D. Lee, S. Y. Park, and D. H. Choi, "Unusual characteristics of diffraction gratings in a liquid crystal cell," Adv. Mater. **14**(13-14), 983–988 (2002).
17. W. Lee and C. C. Lee, "Two-wave mixing in a nematic liquid-crystal film sandwiched between photoconducting polymeric layers," Nanotechnology **17**(1), 157–162 (2006).
18. S. Nersisyan, N. Tabiryan, D. M. Steeves, and B. R. Kimball, "Fabrication of liquid crystal polymer axial waveplates for UV-IR wavelengths," Opt. Express **17**(14), 11926–11934 (2009).
19. D. Xu, G. Tan, S. T. Wu, "Large-angle and high-efficiency tunable phase grating using fringe switching liquid crystal," Opt. Express **23**, 11274–11285 (2015).
20. W. Duan, P. Chen, B. Y. Wei, S. J. Ge, X. Liang, W. Hu, and Y. Q. Lu, "Fast-response and high-efficiency optical switch based on dual-frequency liquid crystal polarization grating," Opt. Mater. Express **6**(2), 597–602 (2016).
21. Y. Zhao, in *Smart Light Responsive Materials – Azobenzene-Containing Polymers and Liquid Crystals*, Y. Zhao, T. Ikeda, ed. (John Wiley & Sons, 2009).
22. M. Warner and E. M. Terentjev, *Liquid Crystal Elastomers* (Oxford University Press, 2007).
23. H. Finkelmann, E. Nishikawa, G. G. Pereira, and M. Warner, "A new opto-mechanical effect in solids," Phys. Rev. Lett. **87**(1), 015501 (2001).
24. P. M. Hogan, A. R. Tajbakhsh, and E. M. Terentjev, "UV manipulation of order and macroscopic shape in nematic elastomers," Phys. Rev. E Stat. Nonlin. Soft Matter Phys. **65**(4), 041720 (2002).
25. Y. Yu, M. Nakano, and T. Ikeda, "Photomechanics: directed bending of a polymer film by light," Nature **425**(6954), 145 (2003).
26. M. Warner and L. Mahadevan, "Photoinduced deformations of beams, plates, and films," Phys. Rev. Lett. **92**(13), 134302 (2004).
27. N. J. Dawson, M. G. Kuzyk, J. Neal, P. Luchette, and P. Palffy-Muhoray, "Experimental studies of the mechanisms of photomechanical effects in a nematic liquid crystal elastomer," J. Opt. Soc. Am. B **28**(8), 1916–1921 (2011).
28. H. Y. Jiang, S. Kelch, and A. Lendlein, "Polymers move in response to light," Adv. Mater. **18**(11), 1471–1475 (2006).
29. U. Hrozhyk, S. Serak, N. Tabiryan, T. J. White, and T. J. Bunning, "Bidirectional photoresponse of surface pretreated azobenzene liquid crystal polymer networks," Opt. Express **17**(2), 716–722 (2009).
30. K. M. Lee, M. L. Smith, H. Koerner, N. Tabiryan, R. A. Vaia, T. J. Bunning, and T. J. White, "Photodriven flexural-torsional oscillation of glassy azobenzene liquid crystal polymer networks," Adv. Funct. Mater. **21**(15), 2913–2918 (2011).
31. M. Camacho-Lopez, H. Finkelmann, P. Palffy-Muhoray, and M. Shelley, "Fast liquid-crystal elastomer swims into the dark," Nat. Mater. **3**(5), 307–310 (2004).
32. H. Zeng, P. Wasylczyk, C. Parmeggiani, D. Martella, M. Burresi, and D. S. Wiersma, "Light-Fueled Microscopic Walkers," Adv. Mater. **27**(26), 3883–3887 (2015).
33. S. Bai and Y. Zhao, "Azobenzene elastomers for mechanically tunable diffraction gratings," Macromolecules **35**(26), 9657–9664 (2002).
34. Y. Zhao, S. Bai, K. Asatryan, and T. Galstian, "Holographic recording in a photoactive elastomer," Adv. Funct. Mater. **13**(10), 781–788 (2003).
35. C. Sanchez, R. Alcala, S. Hvilsted, and P. S. Ramanujam, "High diffraction efficiency polarization gratings recorded by biphotonic holography in an azobenzene liquid crystalline polyester," Appl. Phys. Lett. **78**(25), 3944–3946 (2001).
36. F. Ciuchi, A. Mazzulla, and G. Cipparrone, "Permanent polarization gratings in elastomer azo-dye systems: comparison of layered and mixed samples," J. Opt. Soc. Am. B **19**(11), 2531–2537 (2002).
37. E. Sungur, M. H. Li, G. Taupier, A. Boeglin, M. Romeo, S. Méry, P. Keller, and K. D. Dorkenoo, "External stimulus driven variable-step grating in a nematic elastomer," Opt. Express **15**(11), 6784–6789 (2007).
38. M. Devetak, B. Zupančič, A. Lebar, P. Umek, B. Zalar, V. Domenici, G. Ambrožič, M. Žigon, M. Čopič, and I. Drevenšek-Olenik, "Micropatterning of light-sensitive liquid-crystal elastomers," Phys. Rev. E Stat. Nonlin. Soft Matter Phys. **80**(5), 050701 (2009).
39. V. Domenici, G. Ambrožič, M. Čopič, A. Lebar, I. Drevenšek-Olenik, P. Umek, B. Zalar, B. Zupančič, and M. Žigon, "Interplay between nematic ordering and thermomechanical response in a side-chain liquid single crystal elastomer containing pendant azomesogen units," Polymer (Guildf.) **50**(20), 4837–4844 (2009).
40. M. Gregorc, B. Zalar, V. Domenici, G. Ambrožič, I. Drevenšek-Olenik, M. Fally, and M. Čopič, "Depth profile of optically recorded patterns in light-sensitive liquid-crystal elastomers," Phys. Rev. E Stat. Nonlin. Soft Matter Phys. **84**(3), 031707 (2011).
41. M. Gregorc, H. Li, V. Domenici, G. Ambrožič, M. Čopič, and I. Drevenšek-Olenik, "Optical properties of light-sensitive liquid-crystal elastomers in the vicinity of the nematic-paranematic phase transition," Phys. Rev. E Stat. Nonlin. Soft Matter Phys. **87**(2), 022507 (2013).
42. B. Tašič, W. Li, A. Sánchez-Ferrer, M. Čopič, and I. Drevenšek-Olenik, "Light-induced refractive index modulation in photoactive liquid-crystalline elastomers," Macromol. Chem. Phys. **214**(23), 2744–2751 (2013).
43. M. Gregorc, H. Li, V. Domenici, G. Ambrožič, M. Čopič, and I. Drevenšek-Olenik, "Kinetics of holographic recording and erasure processes in light-sensitive liquid crystal elastomers," Materials (Basel) **5**(12), 741–753 (2012).

#258431 Received 28 Jan 2016; revised 15 Feb 2016; accepted 15 Feb 2016; published 29 Feb 2016

44. J. Küpfer and H. Finkelmann, "Nematic liquid single-crystal elastomers," Makromol. Chem., Rapid. Commun. **12**(12), 717–726 (1991).
45. L. Nikolova, T. Todorov, M. Ivanov, F. Andruzzi, S. Hvilsted, and P. S. Ramanujam, "Polarization holographic gratings in side-chain azobenzene polyesters with linear and circular photoanisotropy," Appl. Opt. **35**(20), 3835–3840 (1996).
46. L. Nikolova and P. S. Ramanujam, *Polarization Holography* (Cambridge University Press, 2009).
47. F. Kahmann, J. Höhne, R. Pankrath, and R. A. Rupp, "Hologram recording with mutually orthogonal polarized waves in $Sr_{0.61}Ba_{0.39}Nb_2O_6$:Ce," Phys. Rev. B Condens. Matter **50**(4), 2474–2478 (1994).
48. M. Xu, D. K. G. de Boer, C. M. van Heesch, A. J. H. Wachters, and H. P. Urbach, "Photoanisotropic polarization gratings beyond the small recording angle regime," Opt. Express **18**(7), 6703–6721 (2010).
49. C. Provenzano, P. Pagliusi, G. Cipparrone, J. Royes, M. Piñol, and L. Oriol, "Polarization holograms in a bifunctional amorphous polymer exhibiting equal values of photoinduced linear and circular birefringences," J. Phys. Chem. B **118**(40), 11849–11854 (2014).
50. C. Oh and M. J. Escuti, "Time-domain analysis of periodic anisotropic media at oblique incidence: an efficient FDTD implementation," Opt. Express **14**(24), 11870–11884 (2006).
51. C. Oh and M. J. Escuti, "Numerical analysis of polarization gratings using the finite-difference time-domain method," Phys. Rev. A **76**(4), 043815 (2007).
52. H. Ono, T. Sekiguchi, A. Emoto, T. Shioda, and N. Kawatsuki, "Light wave propagation and Bragg diffraction in thick polarization gratings," Jpn. J. Appl. Phys. **47**(10), 7963–7967 (2008).
53. F. Zhao, C. Wang, M. Qin, P. Zeng, and P. Cai, "Polarization holographic gratings in an azobenzene copolymer with linear and circular photoinduced birefringence," Opt. Commun. **338**, 461–466 (2015).
54. M. Ishiguro, D. Sato, A. Shishido, and T. Ikeda, "Bragg-type polarization gratings formed in thick polymer films containing azobenzene and tolane moieties," Langmuir **23**(1), 332–338 (2007).

1. Introduction

Optical polarization gratings are periodic holographic structures that are recorded by optical interference patterns at constant intensity but spatially varying polarization states of the optical field [1,2]. They exhibit many interesting properties that can be applied in devices for detection and manipulation of the optical polarization state, such as polarization filters and converters, polarizing beam splitters and polarization-sensitive optical data storage units [3–7]. Liquid crystalline (LC) materials are particularly suitable for fabrication of polarization gratings, because they possess a collective molecular response in combination with a strong optical anisotropy [8,9]. Polarization-responsive recording in liquid crystalline materials is usually based on optical-field-induced reorientation of the mesogenic molecules [10–12]. Another common mechanism that leads to polarization-type LC gratings is holographic or some other type of patterning of surface layers that control the LC alignment [13–20]. In both cases, photoresponse is typically achieved by incorporation of photoisomerizable chemical compounds, mostly azobenzene derivatives [21].

Liquid crystalline elastomers (LCEs) are soft materials that combine liquid crystallinity with rubber elasticity. Light-sensitive LCEs exhibit a huge opto-mechanical response, which is a direct consequence of the specific coupling mechanisms present in these materials [22–24]. Exposed to optical irradiation, they can change size and shape, flip between different shapes, oscillate, or even move on the supporting surface [25–32]. Another interesting feature of light-sensitive LCEs is their strong opto-optical response that is observed as a large photo-induced modification of the optical birefringence. This can be exploited for fabrication of tunable volume-type optical diffraction structures that can be regulated by mechanical strain or by temperature modifications [33–39].

Our recent papers have reported investigations on LCE-based diffraction gratings fabricated by intensity-modulated interference patterns [40–43], while this paper reports on polarization gratings. We show that polarization gratings exhibit a similar magnitude of the diffraction efficiency as intensity gratings. However, in contrast to intensity gratings, they display an unusual dip, i.e. a depression structure, instead of the expected Bragg reflection peak. By extending our theoretical model developed for intensity gratings [40], we show that this dip is a consequence of anisotropic absorption of actinic light during the recording process.

#258431 Received 28 Jan 2016; revised 15 Feb 2016; accepted 15 Feb 2016; published 29 Feb 2016

2. Experiments and results

Single domain side-chain LCE films with 150 μm thickness were prepared according to the two-step "Finkelmann crosslinking procedure" [44]. The polymer back-bone is based on a commercial hydroxymethyl-polysiloxane crosslinked by 1,4-bis (undec-10-en-1-yloxy) benzene. The side-chain moieties are composed of usual rod-like mesogens (4-methoxyphenyl 4-(but-3-en-1-yloxy) benzoate) and light-sensitive azomesogens (1-(4-(hex-5-enyloxy)phenyl)-2-(4-methoxyphenyl) diazene, named J7) attached to the back-bone in the ratio of 9:1. Further details of the sample fabrication and characterization procedures are described elsewhere [39]. In absence of UV illumination, the nematic-paranematic phase transition in this material occurs at T_{c0} = 82°C, where the subscript 0 denotes zero concentration of the *cis* isomers. All measurements were performed at room temperature (23°C).

Optical transmission gratings were recorded by placing the LCE film in the interference field of two expanded laser beams with a wavelength of either λ_r = 351 nm or 364 nm, which resulted in formation of transmission gratings with grating spacing Λ of 1.6 or 1.7 μm, respectively. Recording beams of equal intensity (8 mW/cm^2) entered the film symmetrically with respect to the surface normal. The beams were linearly polarized. Their polarization directions with respect to the nematic director **n** are depicted in Fig. 1. For recording intensity gratings **n** was set parallel to the s-polarization direction and the recording beams were superposed in parallel (s-s or in p-p) polarization combination. For recording of polarization gratings **n** was set at 45° with respect to the s- and p-polarization directions and the recording beams were superposed in perpendicular (s-p) polarization combination. The recording time for all gratings was 10 min.

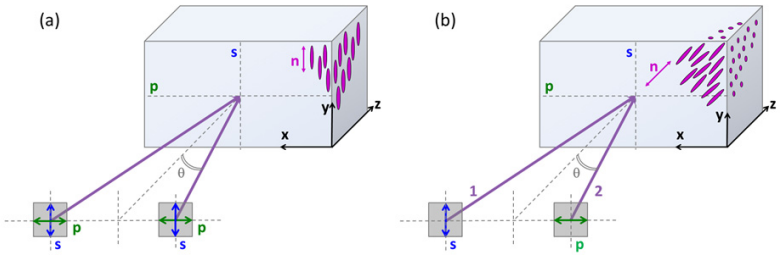

Fig. 1. Schematic drawings of the recording configuration for parallel polarization combination (a) and for perpendicular polarization combination (b), respectively.

Optical diffraction properties of the gratings were examined by a low-power (< 1 mW) laser beam at λ_p = 633 nm, a wavelength to which the LCE is not sensitive. The probe beam was either s or p polarized. The sample was mounted onto a rotation stage and rotated around an axis perpendicular to the plane of incidence. The angular dependence of the intensities I_0, I_{+1} and I_{-1} of the 0th and the ± 1st order diffraction peaks in the vicinity of the Bragg angle θ_B = arcsin(λ_p/2Λ) was measured by photodiode detectors. Intensities of higher diffraction orders were negligible. The (relative) diffraction efficiency was calculated as

$$\eta_i = \frac{I_i}{I_{-1} + I_0 + I_{+1}}, \qquad (1)$$

where i = 1, 0, or + 1. By this definition absorption and scattering losses of the probe beam can be disregarded.

The optical absorbance A of the LCE film at λ_r = 351 nm was so high (> 4) that its dichroism could not be accessed directly. We therefore characterized the dichroism of the azomesogens (J7) incorporated in the film by introducing them into the conventional nematic liquid crystalline mixture E7 (Shijiazhuang Chengzhi Yonghua Display Material Co.).

#258431 Received 28 Jan 2016; revised 15 Feb 2016; accepted 15 Feb 2016; published 29 Feb 2016

Commercial glass cells with a thickness of 7 μm (Instec Inc.) and surface coatings inducing planar LC alignment were filled either with pure E7 or with a mixture of E7 and 1 wt% of J7 and their absorbance as a function of the polarization direction of the linearly polarized incident beam was measured at 351 nm. The results are shown in Fig. 2. Both cells exhibit considerable linear dichroism with maximal absorbance A for the polarization state parallel to the nematic director **n** (Fig. 2(a)). The absorbance difference between both samples (ΔA), which is attributed to the absorbance of the azomesogens, shows a profound number eight shape (Fig. 2(b)). This signifies a strong preferential alignment of the J7 molecules along the direction of **n**. We presume that a similar alignment occurs also when J7 is incorporated into the LCE matrix.

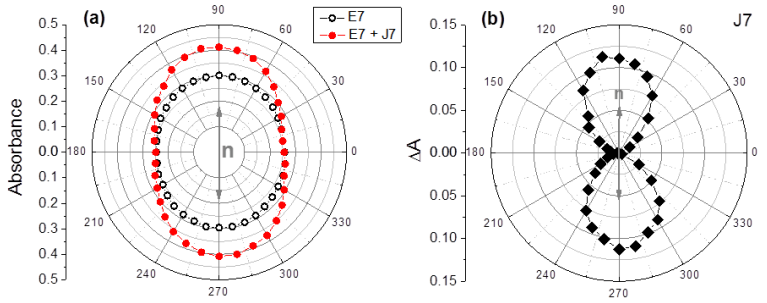

Fig. 2. Absorbance (at 351 nm) of planarly aligned samples of pure E7 and of E7 mixed with 1 wt% of J7 azomesogens as a function of polarization direction of the linearly polarized incident optical beam (a). Difference ΔA between the absorbances of both samples (b). Vertical arrows in the centre denote the orientation of the nematic director **n**.

Figure 3(a) shows the angular dependencies of the diffraction efficiency of the ± 1st diffraction orders as a function of deviation from the Bragg angle $|\theta-\theta_B|$ for gratings recorded either in the s-s or the p-p polarization state combination. The value of $|\theta_B|$ was around 12° (externally measured with respect to normal incidence). The Bragg peak exhibits the FWHMs of ~15° for the grating recorded in the s-s configuration and of ~8° for the grating recorded in the p-p configuration, respectively. This observation indicates that the depth of recording, i.e. the effective grating thickness, is about two times larger for the p-p grating than for the s-s grating [40]. This is a consequence of the weaker absorption (larger penetration depth) of the p-polarized radiation at λ_r = 351 nm as compared to the s-polarized beam. Anyway, the peak diffraction efficiency for the p-p grating is about two times smaller than for the s-s grating, which is a consequence of the fact that the p-p grating was probed by the p-polarized probe beam (at λ_p = 633 nm) while the s-s grating was probed by the s-polarized beam. As discussed in our previous paper, due to the relation between the LC order parameter and birefringence, light polarized perpendicular to the nematic director in general exhibits a lower diffraction efficiency than light polarized parallel to the director [42].

#258431 Received 28 Jan 2016; revised 15 Feb 2016; accepted 15 Feb 2016; published 29 Feb 2016

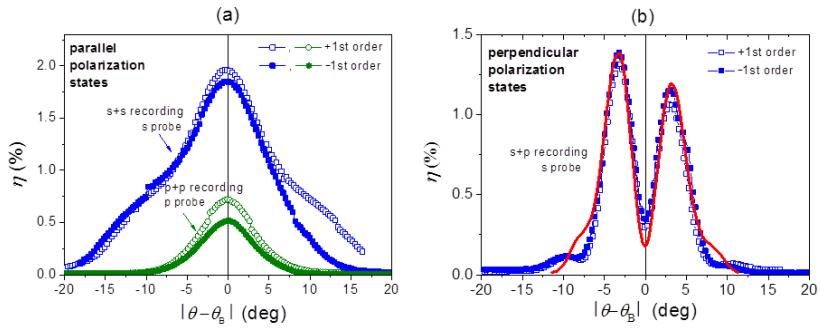

Fig. 3. Diffraction efficiency of the ± 1st diffraction orders as a function of deviation from the Bragg angle for a grating recorded by parallel polarization states (a) and for a grating recorded by perpendicular polarization states (b). Polarization states of the recording and readout (probe) beams are denoted in the images. The red solid line in (b) is the result of a theoretical simulation described in detail in Section 3.

Figure 3(b) shows angular dependencies of the diffraction efficiency for the ± 1st diffraction orders for a grating recorded in the perpendicular (s-p) polarization combination and probed by an s-polarized probe beam. The diffraction efficiency of this grating has a similar magnitude as for the gratings recorded by parallel polarization combinations. However, there exists a striking difference in the observed angular dependence – instead of a peak there is a profound dip observed exactly at the Bragg angle. The depth of the dip varied from sample to sample and from recording to recording, but the dip could always be noticed. We also monitored the angular dependence during decay of the grating due to spontaneous *cis*-to-*trans* back isomerization and found that the magnitude of the diffraction efficiency was decreasing with time, however, its angular dependence including the dip remained the same. This observation confirmed that the dip was not associated with the overmodulation of the gratings.

To verify the universality of the observed behaviour we recorded the grating by using perpendicularly polarized recording beams at another recording wavelength, namely at λ_r = 364 nm. In addition to this, we measured angular dependencies of the diffraction efficiency for p as well as for s polarized probed beams. The results are shown in Fig. 4. One can notice that the dip at the Bragg peak is present also for these cases. In addition, we analysed some LCE samples with different chemical compositions from the one described above and the dip was observed for them too. Hence we propose that the observed behaviour is a general property of polarization gratings recorded in the LCEs. In the following we will show that it can be explained by the large linear dichroism of the material at the recording optical wavelength.

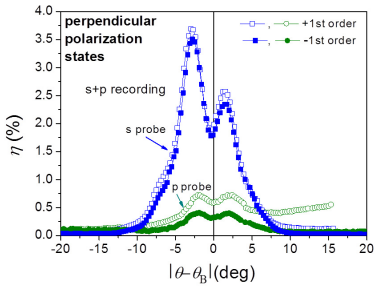

Fig. 4. Diffraction efficiencies of the ± 1st diffraction orders as a function of deviation from the Bragg angle for a grating recorded by perpendicularly polarized recording beams (s + p) and readout by s (squares) and by p polarized (circles) probe beams, respectively.

#258431 Received 28 Jan 2016; revised 15 Feb 2016; accepted 15 Feb 2016; published 29 Feb 2016

3. Theoretical model

Superposition of two coherent optical waves with equal amplitudes but orthogonal polarization states leads to optical interference fields with constant intensity but a periodic spatially varying polarization state [45–47]. At small intersection angles (2θ) of the beams, as it is the case in our recording setup (Fig. 1), the component of the optical field orthogonal to the intersection plane can be neglected (collinear approximation) [48]. Consequently, the superposition of s and p polarized beams results in an interference pattern that is varying between circular and linear polarization as depicted in the top line of Fig. 5. This interference pattern can be decomposed into the superposition of two interference sub-patterns: a sub-pattern of two beams linearly polarized at –45° with respect to the p polarization (direction parallel to **n** in Fig. 1(b) corresponding to extraordinary polarization) and a sub-pattern of two beams linearly polarized at + 45° with respect to the p polarization (direction perpendicular to **n** in Fig. 1(b) corresponding to ordinary polarization) [45,49]. The extraordinary-extraordinary (e-e) and ordinary-ordinary (o-o) sub-patterns are shifted for $\Lambda/2$ along the grating vector (x axis in Fig. 1) [47].

In the LCE material, due to its large linear dichroism, the e-e sub-pattern decreases much faster with sample depth (z axis in Fig. 1) than the o-o sub-pattern. Consequently, the polarization state of the total optical field changes with sample depth and at large depths practically only the o-o sub-pattern subjected to lower absorption survives. Therefore polarization modulation is transformed to intensity modulation. This effect is schematically shown in Fig. 5.

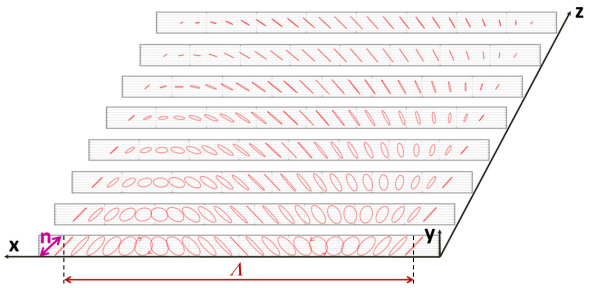

Fig. 5. Optical interference field of s and p polarized optical beams as a function of sample depth (see also Fig. 1). Due to linear dichroism the amplitude of the e-e sub-pattern (polarization at –45° with respect to x axis) decreases with sample depth (z axis) much faster than the amplitude of the o-o sub-pattern (polarization at + 45° with respect to x axis). The direction of nematic director **n** is designated on the left side at the bottom of the image.

Optical absorption in photo-isomerizable materials takes place in a nonlinear manner associated with the difference between the absorption cross sections of the *trans* and the *cis* isomers. *Cis* isomers usually exhibit lower absorption for UV radiation and consequently after the isomerization reaction the material becomes more transparent for the UV light than before it. As a result of this phenomenon, in the beginning of the irradiation process the optical field is present mainly in the surface region of the material. However, with prolonged irradiation, it penetrates deeper and deeper into the volume. This type of "photo-bleaching" is characteristic also for light-sensitive LCEs and was analyzed in one of our previous studies reporting LCE-based optical gratings [40]. However, for intensity gratings considered in Refs [40–43], the anisotropy of optical absorption was not important. If this anisotropy is taken into account, then the rate equation for the relative concentration of the *trans* isomers $c_t = C_t/(C_t + C_c)$, where C_t and C_c denote molar concentrations of *trans* and *cis* isomers (in units of moles/m^3), in [40] is modified to:

$$\frac{dc_t}{dt} = \left[-\gamma_t c_t \left(\sigma_{t,e} |\psi_e|^2 + \sigma_{t,o} |\psi_o|^2 \right) + \gamma_c (1 - c_t) \sigma_c \left(|\psi_e|^2 + |\psi_o|^2 \right) \right] + \frac{(1 - c_t)}{\tau}, \quad (2)$$

#258431 Received 28 Jan 2016; revised 15 Feb 2016; accepted 15 Feb 2016; published 29 Feb 2016

where γ denotes the conversion efficiency from the electronic excited state to the *cis* or *trans* conformation, σ is the absorption cross section, Ψ is a parameter proportional to the optical intensity, and τ is the thermal relaxation time from *cis* to *trans* state. The subscripts t and c denote *trans* and *cis* states and the indices e and o denote extraordinary and ordinary polarized optical fields, respectively. In Eq. (2) it is assumed that light-induced *cis*-to-*trans* back isomerization is independent of the polarization state of the optical field, which is reasonable for the chromophores used in our LCE material. In accordance with Eq. (2), the components of the imaginary part of the uniaxial optical dielectric tensor ε'', can be expressed as:

$$\varepsilon_e^{"} = [c_t \sigma_{t,e} + (1-c_t)\sigma_c]/k_0, \qquad \varepsilon_o^{"} = [c_t \sigma_{t,o} + (1-c_t)\sigma_c]/k_0, \tag{3}$$

where k_0 is the magnitude of the optical wave vector in vacuum.

The above described extensions of the theory presented in [40] were used to calculate depth profiles of the optical intensity for extraordinary and ordinary polarized optical fields for different recording times of the grating. The value of $(\sigma_{t,e}/\sigma_{t,o}) = 2$, in agreement with the measurements shown in Fig. 2 and Fig. 3(a), was used in the calculation. The sample thickness considered in the calculation was 20 μm, which corresponds to the typical effective depth of the gratings for long recording times [40, 41]. The values of all other parameters were set to be the same as in [40]. The optical field was calculated by using a FDTD method-based software package (WOLFSIM) designed for solving the wave equation in periodic structures of arbitrary anisotropic media [50, 51]. The result is shown in Fig. 6. Due to the $\Lambda/2$ shift between the e-e and o-o interference patterns, the maxima of the extraordinarily polarized field coincide with the minima of the ordinarily polarized field and vice versa. Besides this, due to lower absorption, the ordinarily polarized field penetrates deeper into the sample than the extraordinarily polarized field.

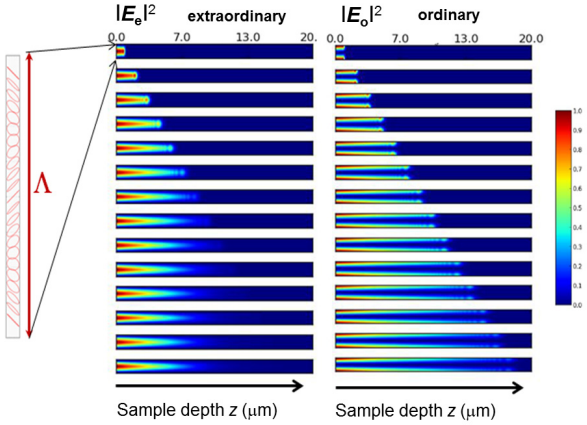

Fig. 6. Calculated intensity profiles of extraordinarily and ordinarily polarized optical fields as a function of sample depth for increasing recording times. The recording time linearly increases from t_r = 10 s (upper segment) to t_r = 140 s (bottom segment). The profile corresponding to one period Λ of the interference pattern is shown in each segment. The ordinarily polarized field penetrates deeper into the sample than the extraordinarily polarized field. Its maxima and minima are shifted for $\Lambda/2$ with respect to the extraordinarily polarized field.

The presence of the UV optical field stimulates a *trans*-to-*cis* isomerization of the azomesogens. This causes a decrease of the nematic order and consequently of birefringence of the LCE medium. At low sample depths, the extraordinary field plays a dominant role in *trans*-to-*cis* isomerization and consequently the birefringence is most profoundly reduced in regions of high intensity of the extraordinary field (red-coloured regions on the left side of

#258431 Received 28 Jan 2016; revised 15 Feb 2016; accepted 15 Feb 2016; published 29 Feb 2016

Fig. 6). At large sample depths, the ordinary field prevails and consequently the birefringence is most profoundly reduced in the regions of high intensity of the ordinary field (red-coloured regions on the right side of Fig. 6). Due to the $\Lambda/2$ spatial shift of these regions, the modulation of the birefringence changes its sign as a function of the sample depth. The spatial dependence of the anisotropy of the real part of the optical dielectric tensor $\Delta\varepsilon$ can be described as [40]:

$$\Delta\varepsilon(x,z) = \varepsilon_e^{'} - \varepsilon_o^{'} = \varepsilon_a + \Delta\varepsilon_1(z)\cos(K_g x), \tag{4}$$

where $\varepsilon_e^{'}$ and $\varepsilon_o^{'}$ denote extraordinary and ordinary components of the real part of the optical dielectric tensor, ε_a is the average anisotropy, $\Delta\varepsilon_1(z)$ is the modulation of the anisotropy that depends on the sample depth z, and $K_g = 2\pi/\Lambda$ is the magnitude of the grating vector. The calculated dependence of $\Delta\varepsilon_1(z)$ for some selected recording times is shown in Fig. 7. One can notice the change of the sign at a depth of about 30% of the sample thickness. The oscillations at the rear side of the sample are the consequence of boundary conditions and limited mesh size.

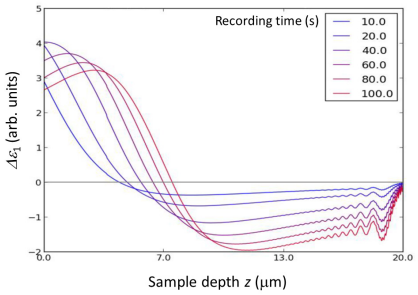

Fig. 7. Modulation of anisotropy of the real part of the optical dielectric tensor as a function of sample depth for different recording times. The relative recording times are denoted in the inset. The resulting calculated angular dependence of the diffraction efficiency of the ± 1st diffraction orders for t_r = 100 s is shown as a thick solid line in Fig. 3(b).

The change of the sign of $\Delta\varepsilon_1(z)$ with sample depth causes destructive interference between the diffraction field of the probe beam generated in surface region of the sample and the diffraction field generated in inner parts of the sample. This effect is most pronounced when the probe beam enters the sample at the Bragg angle θ_B. For a weakly diffracted beam the diffraction efficiency of the ± 1st diffraction orders in the vicinity of θ_B can be expressed as [47]:

$$\eta \propto \left| \int_0^L \Delta\varepsilon_1(z) e^{iK_g \Delta\theta z} dz \right|^2, \tag{5}$$

where L is the sample thickness and $\Delta\theta = \theta - \theta_B$ measures a deviation from the Bragg angle. The calculated angular dependence of the diffraction efficiency $\eta(\theta)$ (limited to -0.2 rad $< \theta <$ + 0.2 rad) corresponding to the longest recording time considered in Fig. 7 is shown as a red solid line in Fig. 3(b). A profound dip with minimum at $\theta = \theta_B$ is evident. Also in general, a good agreement between the calculated and the measured dependence of $\eta(\theta)$ can be noticed. The largest variations in the observed angular behavior appear in the value of $\eta(\theta = \theta_B)$ (Fig. 4). As follows from Eq. (5), this value is determined by $\int_0^L \Delta\varepsilon_1(z)dz$, which depends on the details of the evolution of $\Delta\varepsilon(x,z)$ during the recording process. Further experiments employing varying recording times are needed to resolve these details.

#258431 Received 28 Jan 2016; revised 15 Feb 2016; accepted 15 Feb 2016; published 29 Feb 2016

Having applications in mind, one might wonder how to avoid a detrimental dip at the Bragg angle. As follows from our study, one simply should use either recording wavelengths for which the material exhibits low linear dichroism or employ parallel polarization states. On the other hand, the dip might also be advantageous, e.g., in multiplexing of the usual intensity gratings with polarization gratings. Here, the former can be optimally read out at the Bragg angle whereas the latter in off-Bragg geometry, therefore any "cross-talk" effects can be reduced.

4. Conclusions

Our results demonstrate that a strong linear dichroism at the actinic optical wavelength, which is characteristic for light-sensitive LCEs and also for many other kinds of light-sensitive liquid crystalline materials, can drastically influence the volume-type polarization holographic recording in photo-responsive media. However, up till now this effect was mostly neglected [46, 52]. In combination with strongly nonlinear recording kinetics associated with photo-bleaching, dichroism can lead to diffractive structures exhibiting various unusual phenomena, such as a profound minimum of the diffraction efficiency at the Bragg angle, which was the subject of our present investigation.

Other features that are worth being studied in LCE-based polarization gratings are polarization properties of the diffracted light and the effect of mechanical strain and temperature on these properties [53]. Another open problem that can be conveniently investigated by analysis of optical polarization gratings, is photo-induced alignment in the LCE materials [36, 54]. Besides this, optical polarization gratings recorded in the LCE media can also open up various new challenges for construction of polarization-sensitive diffractive optical elements that can be regulated by different external stimuli, in particular by mechanical strain.

The diffraction efficiency of a few percent, typically observed in our experiments, is usually too low for practical applications. We want to emphasize that this work focused on a fundamental explanation of the reported phenomenon, and for that reason the same LCE material was used as in our previous studies. This approach allowed us to use material parameters deduced from these studies for our numerical simulations and enhances their soundness. However, the investigated LCE material is far from being optimised from the point of view of diffraction efficiency. As shown in our recent paper, small variations of the chemical structure of the azomesogen moiety and/or suitable clamping of the LCE film can improve the diffraction efficiency for one order of magnitude [42]. In addition, further improvements are easily possible by optimizing the recording optical wavelength (with respect to the absorption spectrum of the material), so that the effective thickness of the grating is increased and consequently diffraction occurs in the two-wave Bragg diffraction regime. Another important aspect for applications is also to reduce the grating spacing to about Λ~500 nm, which is an open problem with LCE gratings that needs to be investigated in the future.

Acknowledgments

We acknowledge financial support in the frame of the National Research Program of Slovenia P1-0192 and the projects of bilateral cooperation BI-AT/09-10-009 and BI-AT/11-12-015. We are grateful for supporting scientific exchange by travel grants in the frame of OEAD-WTZ SI19/2009 and OEAD-WTZ SI-07-2011. Funding by the Open Access Publishing Fund of the University of Vienna is acknowledged.

#258431 Received 28 Jan 2016; revised 15 Feb 2016; accepted 15 Feb 2016; published 29 Feb 2016